Physics of Fluids

RESEARCH ARTICLE | DECEMBER 06 2005

Aspect ratio effects in quasi-two-dimensional turbulence

K. Ngan; D. N. Straub; P. Bartello

Check for updates

Physics of Fluids 17, 125102 (2005)
https://doi.org/10.1063/1.2139685

View Online
Export Citation
CrossMark

06 July 2023 14:07:29

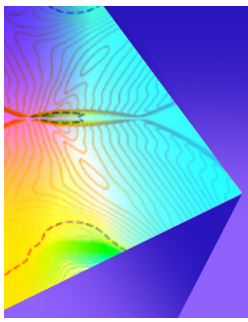
Physics of Fluids
Special Topic: Shock Waves
Submit Today!

AIP Publishing

Aspect ratio effects in quasi-two-dimensional turbulence

K. Ngan,[a] D. N. Straub, and P. Bartello[b]
Department of Atmospheric and Oceanic Sciences, McGill University, Montréal, Québec H3A 2K6, Canada

(Received 9 February 2005; accepted 20 September 2005; published online 6 December 2005)

The influence of the aspect ratio on the three-dimensionalization and subsequent saturation of freely decaying two-dimensional turbulence is studied numerically. We show that the aspect ratio strongly affects the saturation level of the perturbation and its feedback on the base flow. The saturation level scales linearly with the aspect ratio, as does the total damping exerted by the perturbation. In spectral space the feedback yields a positive eddy viscosity at large scales and a small eddy viscosity at small scales. A surprising result is the persistence of coherent vortices even after the saturation of the perturbation. © *2005 American Institute of Physics*. [DOI: 10.1063/1.2139685]

I. INTRODUCTION

In the first part of this study (hereafter P1),[1] the three-dimensionalization of freely decaying two-dimensional (2D) turbulence was studied numerically. It was shown that the hyperbolic instability of steady mixing layers generalizes to unsteady flow, and that the growth rate of the perturbation can be estimated with a local, "pressureless" analysis. Following previous studies of hyperbolic instability, linear dynamics and linear growth rates were emphasized. The robustness of the steady, pressureless analysis is a key result: local growth rates that neglect pressure effects and the time dependence of the base flow provide a surprisingly good estimate of the initial perturbation growth.

At later times this linear picture breaks down. In this regime new questions arise. Two come immediately to mind: (i) How large does the perturbation grow? (ii) What is the effect of the perturbation on the base flow? In this paper these questions are examined numerically by adding a small 3D perturbation to an unsteady, 2D base flow. The saturation level of the perturbation is determined from ensemble averages; energy exchanges between the base flow and the perturbation are quantified using transfer functions and energy spectra.

The saturation level and the perturbation-base flow interaction represent different perspectives on the same phenomenon—the three-dimensionalization of a 2D flow. Traditionally, however, the saturation level has been the concern of (nonlinear) stability theory, while the perturbation-base flow interaction, as encapsulated in a quantity like the eddy viscosity, has been left to turbulence modeling. The goal of the present work is to (re)examine these quantities in light of our knowledge of the linear, pressureless growth.

We organize our numerical results around a single nondimensional parameter, the aspect ratio, ε_a. The aspect ratio governs the perturbation magnitude, with smaller ε_a corresponding to more 2D flow. We show that, in agreement with theoretical predictions,[2] the saturation level scales linearly with ε_a for $\varepsilon_a \leqslant \frac{1}{2}$. We also show that the feedback of the perturbation on the base flow decreases significantly as $\varepsilon_a \to 0$.

There is limited understanding of aspect ratio effects in homogeneous turbulence. Classical turbulence phenomenology, which assumes isotropy,[3,4] is strictly applicable only to the inertial ranges of 2D and 3D turbulence. For an anisotropic 3D flow traces of 2D behavior may persist at large scales. Although one expects the flow to isotropize between $\varepsilon_a=0$ and $\varepsilon_a=1$, the value of this critical aspect ratio is not obvious a priori. One of our central findings is that anisotropy may persist—quasi-2D vortices survive beyond the saturation of the perturbation—for aspect ratios less than unity. At our highest resolution the vortices survive for $\varepsilon_a \leqslant \frac{1}{2}$.

Aspect ratio effects have been studied in the context of 3D turbulence with small-scale forcing.[5,6] An inverse energy cascade has been observed for small ε_a and certain types of forcing[5]; with rotation the transfer of energy to large scales diminishes as ε_a is decreased.[6] The forced and unforced problems, however, are fundamentally different. In the absence of forcing, an inverse energy cascade cannot be maintained. Consequently we focus on the forward energy cascade.

Although theoretical considerations constitute the primary motivation for our study, there are also practical reasons for examining aspect ratio effects. Geophysical flows are characterized by a small aspect ratio[7] (for large-scale flows, $\varepsilon_a \sim 0.1$ in the atmosphere and $\varepsilon_a \sim 0.01$ in the ocean). Moreover, as they are approximately 2D to leading order, one often employs "balanced" models that effectively filter out the "unbalanced" or 3D modes. For these reasons the study of the aspect-ratio dependence of the 3D perturbation, and in particular the feedback on the 2D base flow, may have implications for geophysical modeling. Parametrizing the effects of the "unbalanced motion" remains an outstanding problem. The flows considered in this paper—which neglect stratification, rotation and forcing—obviously represent a severe idealization; nonetheless, they may serve as prototypes for more realistic ones.

Since this paper is closely related to P1, the numerical formulation (Sec. II) and the hyperbolic instability for $\varepsilon_a < 1$ (Sec. III) are succinctly described. The main results

[a]Electronic mail: kngan@zephyr.meteo.mcgill.ca
[b]Also at Department of Mathematics and Statistics, McGill University.

06 July 2023 14:07:29

 © 2005 American Institute of Physics

are contained in Secs. IV and VI, the former concerned with the saturation level as a function of ε_a, the latter with the feedback on the base flow, as measured by eddy viscosities[8–10] and the spectral energy transfer from the 3D to 2D modes. Section V is an interlude of sorts that considers an important constraint on the saturation level, the persistence of quasi-2D vortices ("vortex tubes") and the "return to isotropy." We summarize our results in Sec. VII.

II. NUMERICAL FORMULATION AND PROCEDURE

We use the numerical model of P1: a triply periodic, cylindrically truncated, pseudospectral model of the homogeneous, 3D Navier-Stokes equations. In vorticity form

$$\frac{\partial \boldsymbol{\omega}}{\partial t} + \boldsymbol{v} \cdot \boldsymbol{\nabla} \boldsymbol{\omega} = \boldsymbol{\omega} \cdot \boldsymbol{\nabla} \boldsymbol{v} - \nu \nabla^8 \boldsymbol{\omega}.$$

The variables are dimensional, and the initial conditions chosen such that the eddy turnover time is of order 1. ν is sufficiently small that the base flow energy decays negligibly over the linear growth phase (for $\varepsilon_a = 1$ the decay is of the order of 2%). See P1 for a complete description of the model and the parameter values.

∇^8 hyperviscosity is employed so as to minimize finite-resolution effects. With regular Laplacian viscosity, the 3D perturbation does not grow for our thinnest domain of $180^2 \times 8$ points because a significant fraction of the modes lie in the dissipation range—the effective Reynolds number is too low. Nonetheless, we are confident in the robustness of our results. At higher vertical resolution ($\varepsilon_a > 1/3$) the long-time results of Sec. IV are qualitatively similar. For the thinnest domains there is much better agreement with second- and third-order hyperviscosity. While there are some quantitative variations among runs with different viscous terms, they are no greater than those associated with different basic states.

In P1 we used an isotropic domain with N^3 collocation points. In the present study we consider an anisotropic domain, a squished box whose horizontal dimension L_0 exceeds its vertical dimension H_0. Although the domain is anisotropic some freedom exists in the definition of the computational grid. Most of our results were obtained with an isotropic grid wherein the maximum vertical wave number equals the maximum horizontal wave number (but the minimum wave numbers differ). The collocation grid consists of $N_h^2 \times N_v$ points with $\varepsilon_a := N_v/N_h$ and $\Delta x = \Delta y = \Delta z$; equivalently, $\varepsilon_a := H_0/L_0$ with $L_0 = 2\pi$, $H_0 = \varepsilon_a L_0$, with $H_0 = L_0$ for an isotropic domain.

For one of our calculations (Fig. 4), an anisotropic grid was used in order to achieve smaller aspect ratios. With the anisotropic grid, the vertical wave numbers are scaled by a factor of $1/\varepsilon_a$, so that the maximum horizontal wave number no longer equals the maximum vertical wave number, i.e., $\Delta z = \varepsilon_a \Delta x = \varepsilon_a \Delta y$. N_h^3 points are used and the vertical viscosity is scaled by a factor of ε_a^8 so as to keep the dissipation constant at the largest wave number.

The procedure follows P1 (cf. Fig. 1 therein): small-amplitude 3D perturbations are added to 2D basic states, the basic states being generated from long, unforced simulations (hereafter "intermittent" or "more intermittent") or, occasionally, from long simulations with temporally random forcing (hereafter "nonintermittent" or "less intermittent"). The amplitude of the perturbation is determined by specifying its energy as a fraction, $r_{3D/2D}$, of the basic-state energy. The forcing is never applied after the perturbation is added (see P1 for a description of the forcing). Multiple realizations (typically 8) are generated for each set of parameters; each realization corresponds to a different basic state (i.e., different random initial conditions). Unless stated otherwise, $r_{3D/2D} = 0.00001$, $N_h = 180$, and the basic state is intermittent.

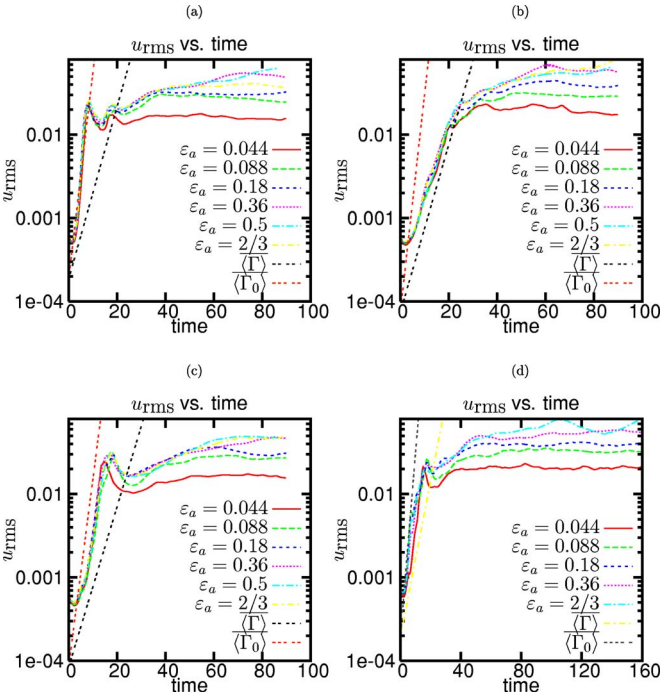

FIG. 1. Evolution of $u_{\rm rms}$ for several different ε_a. Each panel corresponds to a different intermittent basic state. $\langle\Gamma\rangle$ and $\langle\Gamma_0\rangle$ are obtained from a least-squares fit over $t \in [2, 20]$.

The decomposition of the velocity field into base flow and perturbation is effected by spectral filtering: the 2D base flow $\boldsymbol{U}$ corresponds to the $k_z = 0$ modes, and the 3D perturbation $\boldsymbol{u}$ to the $k_z \neq 0$ modes. The full 3D velocity $\boldsymbol{v} := \boldsymbol{U} + \boldsymbol{u}$. Diagnostics will be defined as needed.

III. HYPERBOLIC INSTABILITY FOR $\varepsilon_a < 1$

In P1 we showed that freely decaying 2D turbulence three-dimensionalizes through the hyperbolic instability. Physically, the instability arises from straining of the 3D perturbation by the 2D base flow—horizontal vorticity, in the form of so-called rib vortices, is generated. Mathematically, the hyperbolic instability may be analyzed with a "pressureless" approximation. From the linearized perturbation equations

$$\frac{\partial \boldsymbol{u}}{\partial t} + \boldsymbol{U} \cdot \boldsymbol{\nabla} \boldsymbol{u} = -\boldsymbol{\nabla} p - \boldsymbol{u} \cdot \boldsymbol{\nabla} \boldsymbol{U}, \quad \boldsymbol{\nabla} \cdot \boldsymbol{u} = 0,$$

the horizontal pressure gradient may be neglected if the horizontal scale of the flow is large compared to the vertical scale, that is, if $\epsilon < 1$, $\epsilon := H/L$ being the ratio of character-

06 July 2023 14:07:29

istic vertical and horizontal scales. More precisely,

$$\frac{|\nabla_h p|}{|\mathbf{u}\cdot\nabla\mathbf{U}|} \sim O(\epsilon^2). \tag{1}$$

In this limit the perturbation equation reduces to the compact form

$$\frac{D\boldsymbol{u}_h}{Dt} = -\boldsymbol{u}_h\cdot\nabla\boldsymbol{U}, \tag{2}$$

where $D/Dt=\partial/\partial t+\boldsymbol{U}\cdot\nabla$. This equation is analogous to the equation for a material line element. Therefore, just as a large-scale random-strain field will cause a material line element to stretch, so too will a turbulent 2D base flow $\boldsymbol{U}$ cause the 3D perturbation $\boldsymbol{u}$ to grow. These predictions hold in an isotropic domain.[1]

In this paper we focus on consequences of the hyperbolic instability. To this end, it is useful to verify explicitly that the hyperbolic instability behaves similarly in an anisotropic domain. From the pressureless analysis the underlying mechanism should be essentially 2D, implying that the hyperbolic instability is independent of the aspect ratio. This is most easily seen with the linear growth rate, which is determined by (statistical) properties of the base flow. Assuming a separation of time scales between the base flow and the perturbation, and neglecting spatial and temporal variations, the growth rate may be estimated as $\Gamma_0=\pm\frac{1}{2}\sqrt{\sigma^2-\omega^2}$ or $\Gamma=\pm\frac{1}{2}\sqrt{\sigma^2-(\omega-2\dot{\phi})^2}$, where $\sigma=[(U_x-V_y)^2+(V_x+U_y)^2]^{1/2}$ and $\omega=V_x-U_y$ denote the strain and vorticity of the base flow, and $-\dot{\phi}$ is the rotation rate of the strain axes in the Lagrangian frame. See P1 for details.

Figure 1 shows the time evolution of the rms average of the 3D perturbation, u_{rms}, for an intermittent basic state and several different ε_a. As in P1 the growth rates are bracketed by Γ and Γ_0, i.e., there is exponential growth for $t\lesssim t_{\mathrm{nlin}}\sim 20$, the precise value of t_{nlin} being realization dependent. While the different ε_a curves do not coincide exactly—there is some scatter, on the order of 10%, among the different ε_a in each panel—a systematic trend cannot be discerned, and the scatter is dwarfed by variations from one basic state to another: the (linear) growth rate is independent of aspect ratio.

For $t>t_{\mathrm{nlin}}$ differences between the ε_a are visible. The perturbation attains a larger value as ε_a is increased (cf. Fig. 1(d), which shows simulations extended to $t\sim 160$). Sections IV–VI describe ramifications of this observation.

IV. SATURATION LEVEL

Rigorous bounds on the nonlinear saturation of a perturbation have been obtained for certain problems.[11] They cannot be straightforwardly obtained for nonparallel flows. Yet even without rigorous bounds, estimates on the aspect-ratio dependence of the saturation level can be derived. A simple scaling argument yields the saturation level of the 3D perturbation, u_{sat}.[2]

The pressureless analysis, which describes the initial growth, assumes the time scale of the 2D base flow, T_{2D}, is long compared to the time scale of the 3D perturbation, T_{3D}.[1]

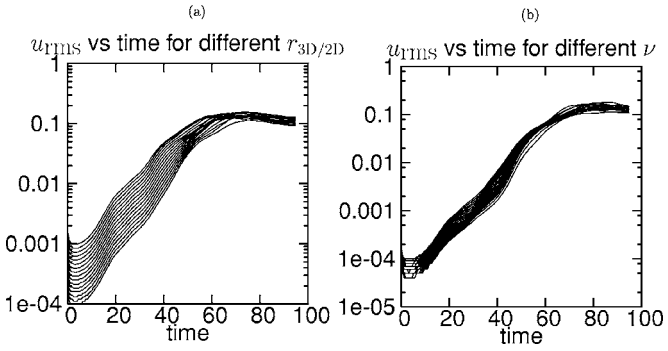

FIG. 2. Robustness of the saturation level with respect to (a) perturbation amplitude; (b) viscosity. $N_h=N_v=72$ and $\varepsilon_a=1$.

This time-scale separation should break down after the final transition. Consequently one expects the flow to isotropize at all scales, i.e.

$$T_{\mathrm{2D}} \sim T_{\mathrm{3D}}. \tag{3}$$

(One may associate this process with, for example, shear instability in the vertical.) From (3) a scaling expression for u_{sat} follows. Assuming

$$T_{\mathrm{2D}} \sim \frac{U}{L}, \quad T_{\mathrm{3D}} \sim \frac{u}{H}, \qquad L\sim L_0, \quad H\sim H_0, \tag{4}$$

then at saturation

$$u_{\mathrm{sat}} \sim \varepsilon_a U_{\mathrm{sat}}, \tag{5}$$

if $T_{\mathrm{2D}}\sim T_{\mathrm{3D}}$. That is, the saturation level scales linearly with the aspect ratio of the domain. We let t_{sat} denote the (approximate) time at which the onset of saturation occurs. Typically $t_{\mathrm{sat}}\gg t_{\mathrm{nlin}}$.

This argument is based on the hyperbolic instability, but not limited to it. All that is required is that the growth mechanism be 2D and associated with the advective time scale, and that the 3D motion be determined by an overturning timescale. There is no restriction on the initial conditions.

The scaling expression (5) has a simple physical interpretation: the saturation level decreases as $\varepsilon_a\to 0$ because the flow becomes more 2D. As the aspect ratio is decreased, the structure of the vorticity field approaches that of decaying 2D turbulence. For larger aspect ratios the vorticity field is more isotropic and the 3D perturbation accordingly larger.

We wish to examine the validity of (5). Once a criterion for u_{sat} is chosen this is a simple numerical exercise—the runs considered in Sec. III can be analyzed directly. But before doing so it is useful to consider a preliminary question: is the saturation level a meaningful concept in practice? If the saturation level is sensitive to the amplitude of the perturbation, or to minor variations in the structure of the flow, then it makes no sense to speak of the saturation level as a function of the aspect ratio.

Several robustness tests are summarized in Fig. 2. Figure 2(a) shows that the saturation level is largely independent of the perturbation amplitude. For a given basic state, varying

06 July 2023 14:07:29

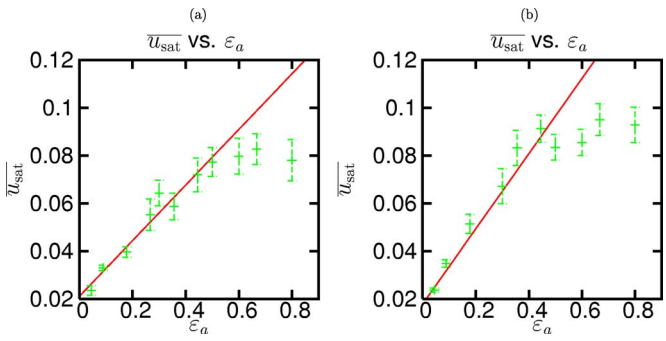

FIG. 3. Ensemble-averaged saturation levels for (a) intermittent and (b) less-intermittent base flows. Each data point was obtained from an ensemble of eight realizations. Points for which $\varepsilon_a > \frac{1}{2}$ are excluded from the fit.

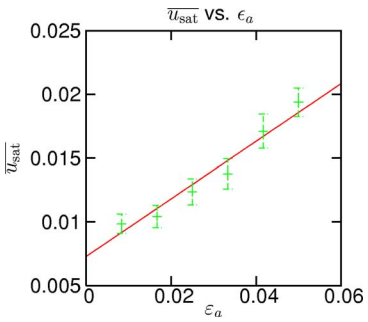

FIG. 4. Aspect-ratio dependence of $\overline{u_{\rm sat}}$ for $\varepsilon_a \lesssim 0.05$. Intermittent base flow with $N_h = 120$ and an anisotropic grid. Each data point was obtained from an ensemble of eight realizations.

$r_{\rm 3D/2D}$ by a factor of 100 (so that the initial amplitude of the velocity perturbation varies by a factor of 10), does not produce a systematic drift in the saturation level, however one chooses to define it. Figure 2(b) shows that the saturation level depends only weakly on the viscosity coefficient, which also varies by a factor of 100. Together, these results imply that for a given basic state the saturation level is a function only of the aspect ratio. Below we shall see that many aspects of the perturbation-base flow interaction are independent of the basic state.

Since the flow is decaying the saturation level cannot be defined unambiguously. For convenience we use $u_{\rm sat} := \max u_{\rm rms}$. This is a reasonable definition inasmuch as the saturation level should be related to the maximum value of the perturbation. [The length T of the simulations is sufficiently long that $u_{\rm sat} > u_{\rm rms}(T)$. For $\varepsilon_a \sim 0.8$, $T \sim 150$, and $u_{\rm rms}(T)/u_{\rm sat} \sim 0.85$.] Nevertheless other definitions are possible. The present definition may represent an overestimate if the $u_{\rm rms}$ curves converge at large times (cf. Fig. 2). An alternative definition is discussed below.

Figure 3 depicts the aspect ratio dependence of $u_{\rm sat}$ for intermittent and less-intermittent base flows. The ensemble average, $\overline{u_{\rm sat}}$, scales linearly with ε_a for $\varepsilon_a \lesssim \frac{1}{2}$, the error bars corresponding to the standard error of the ensemble. The scaling breaks down for $\varepsilon_a \gtrsim \frac{1}{2}$ because the estimates $L \sim L_0$, $H \sim H_0$ are inaccurate (see Sec. V for discussion of the significance of the value $\varepsilon_a = \frac{1}{2}$). If L_0 is fixed, as in our simulations, then $\overline{u_{\rm sat}}$ may assume its maximum value for $\varepsilon_a < 1$. Typically $L < L_0$, so saturation corresponds to $H \sim L$, not $H \sim L_0$ [cf. (5)]. For this reason the $\overline{u_{\rm sat}}(\varepsilon_a)$ curve flattens out.

There is also linear scaling for other definitions of the saturation level. Choosing the saturation level as the final value of $u_{\rm rms}$, $\tilde{u}_{\rm sat} := u_{\rm rms}(T_f)$, where $T_f \sim 90$ is the largest time common to all realizations, linear scaling is recovered (not shown). Although this definition could be problematic, inasmuch the flow might not have saturated by T_f, most runs are sufficiently long to circumvent this concern. [Realizations for which $u_{\rm rms}(T_f) = \max u_{\rm rms}$ are excluded from the ensemble average.] $u_{\rm sat}$ and $\tilde{u}_{\rm sat}$ yield qualitatively similar results. The precise value of the saturation level is, however, sensitive to the definition.

An isotropic grid was used for the calculations of Fig. 3. This limits the range of ε_a that can be attained; with an anisotropic grid smaller ε_a can be achieved. Ensemble results covering the range $0.01 \lesssim \varepsilon_a \lesssim 0.1$ have been obtained, at lower resolution ($N_h = 120$), using the anisotropic grid (Fig. 4). The linear scaling seen in Fig. 3 extends to smaller ε_a. When there is sufficient vertical resolution (i.e., $N_v \gtrsim 8$), the isotropic and anisotropic grids yield nearly identical saturation levels (not shown).

V. RETURN TO ISOTROPY

Although it is natural to define the saturation level using $u_{\rm rms}$, (5) suggests that $u_{\rm sat}/U_{\rm sat}$ may be a more appropriate scaling variable. Since, however, $\alpha := u_{\rm rms}/U_{\rm rms}$ equilibrates more slowly than $u_{\rm rms}$, fluctuations are larger. We have therefore used $\overline{u_{\rm sat}}$ to confirm the validity of (5).

Yet α is of interest in its own right. α characterizes the isotropization: initially the flow is highly anisotropic and α small; as the perturbation grows the flow isotropizes and α increases. Naively one might expect $\alpha \to 1$ at large times for all ε_a. But saturation of the perturbation does not necessarily imply complete isotropization. For some ε_a the quasi-2D vortices present in the initial conditions may persist.

The location of the shoulder in Fig. 3, ε_c, follows from the number of surviving vortices. Prior to the final transition, the base flow approaches a state dominated by two large vortices, one positive and one negative (cf. P1, Figs. 3 and 5). This holds for the more- and less-intermittent basic states. In this limit $L \sim \frac{1}{2}L_0$ and $\overline{u_{\rm sat}} \sim 2\varepsilon_a U$, implying that the saturation level will be maximized for $\varepsilon_c \sim \frac{1}{2}$. ε_c plays a distinguished role in the interpretation of our results.

With the foregoing in mind, let us now consider the long-time evolution of α. (The length of the runs precludes ensemble averaging.) Figure 5 shows the time evolution of α for $\varepsilon_a \in [2/45, 1]$.[12] For $\varepsilon_a < 8/9$, there appears to be incomplete isotropization, i.e., $\alpha_{\rm sat} < 1$. Indeed $\alpha_{\rm sat} \lesssim 0.1$ for $\varepsilon_a \leqslant \frac{1}{2}$. The flow remains anisotropic even after the perturbation has saturated.

For cases in which complete isotropization occurs, i.e., $\varepsilon_a = 8/9$ and $\varepsilon_a = 1$ in Fig. 5, several hundred eddy turnover times are required for α to approach unity. (The eddy turnover time remains $O(1)$ over the course of the simulations.) So the return to isotropy is relatively slow. Nonetheless, it appears as though α relaxes exponentially towards $\alpha = 1$.

06 July 2023 14:07:29

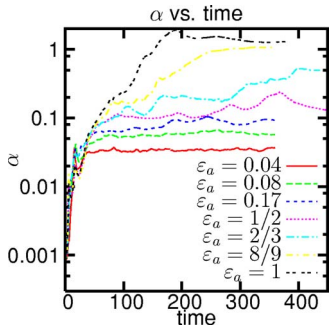

FIG. 5. $\alpha := u_{\rm rms}/U_{\rm rms}$ vs time using the basic states of Fig. 1(d).

This is consistent with phenomenological theories of anisotropic turbulence[3] and with closure calculations.[13,14] Exponential relaxation is not observed for $\varepsilon_a < \varepsilon_c$ because of the presence of coherent vortices. Complete isotropization will eventually occur via viscous effects, but the approach to isotropy should be algebraic in time.

One cannot conclude that $\varepsilon_a \sim 8/9$ sharply divides runs that isotropize from runs that do not. Indeed, shorter runs with other basic states indicate that $\alpha \to 1$ for $\varepsilon_a \sim 2/3$ (not shown). Thus we claim that isotropization does not occur for $\varepsilon_a \leqslant \frac{1}{2}$. In this range extended simulations do not isotropize, for either basic state, on the time scales under consideration. This conclusion is supported by the ensemble runs of Fig. 3. For $\varepsilon_a \leqslant \frac{1}{2}$ candidates for complete isotropization cannot be found; for $\varepsilon_a > \frac{1}{2}$ strong growth can occur for $t \lesssim 100$. These results suggest that $\varepsilon_c \sim \frac{1}{2}$ defines a critical value not only for the validity of the linear scaling, but also for the isotropization of the base flow. The flow should be isotropic when the 3D perturbation has reached its maximum value; $\varepsilon_a = \varepsilon_c$ represents an isotropization criterion for the anisotropic base flow, i.e., it corresponds to an equivalent isotropic domain. Since the 2D flow (and thus L) depends only weakly on resolution (cf. P1, Sec. III B), one expects ε_c to be approximately the same at higher resolution.

Vertically averaged vertical vorticity fields indicate incomplete isotropization for some values of ε_a. Figure 6 shows snapshots at the late time $t \sim 180$. For clarity the zero contour has been excluded (this accounts for the presence of sizeable regions between the vortices that are devoid of contours). Quasi-2D vortices, which imply anisotropy, can be seen for $\varepsilon_a \leqslant \varepsilon_c = \frac{1}{2}$ [panels (a)-(c)]; for $\varepsilon_a = 1$ [panel (d)] they disappear around $t \sim 150$, whereupon $\alpha_{\rm sat} \to 1$.

The size of the (surviving) vortex tubes decreases as ε_a is increased. We have attempted to quantify this through computations of the integral wave number,

$$k_{\rm 2D} = \frac{\sum_0^{K_h} k_h E_{\rm 2D}(k_h)}{\sum_0^{K_h} E_{\rm 2D}(k_h)}. \tag{6}$$

$k_{\rm 2D} \sim 2$ irrespective of ε_a, which means that the 2D energy [cf. (9)] is localized at large scales whether coherent vortices are present or not. So $k_{\rm 2D}$ is of minimal use as a diagnostic of the size of the vortex cores. But it does underscore the significance of $\varepsilon_c = \frac{1}{2}$ (for both basic states).

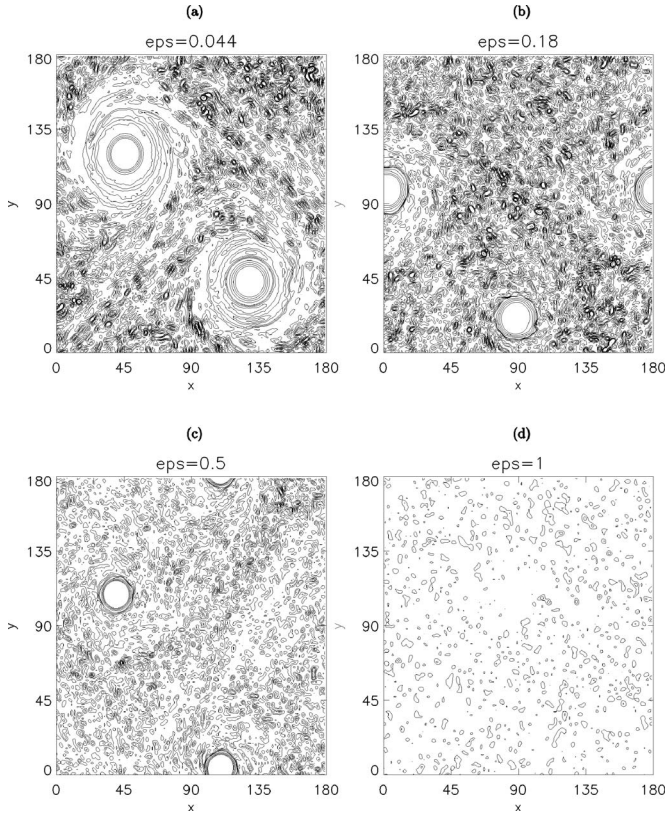

FIG. 6. Vertically averaged ($k_z = 0$) vertical vorticity fields at $t \sim 180$ corresponding to Fig. 5. The same set of contour levels is used for each panel; for clarity the zero contour is excluded. (a) $\varepsilon_a = 0.044 (180^2 \times 8)$; (b) $\varepsilon_a = 0.18 (180^2 \times 32)$; (c) $\varepsilon_a = 0.5 (180^2 \times 90)$; (d) $\varepsilon_a = 1 (180^3)$.

At lower resolution ($N_h = 120$) the return to isotropy remains slow (not shown). Again, many eddy turnover times are required for the vortex tubes to disappear. In this case, too, there is complete isotropization for $\varepsilon_a \gtrsim \varepsilon_c = \frac{1}{2}$.

Anisotropy, in the sense of $\alpha < 1$, does not necessarily invalidate the linear scaling (5), which assumes $T_{\rm 2D} \sim T_{\rm 3D}$. Figure 7 shows time series of $\beta := \omega_h/\omega_z$, where ω_h and ω_z denote the rms horizontal and vertical vorticities. In order for the linear scaling argument to hold, we require $\beta \sim 1$ for all ε_a. While this is not exactly true—$\beta < 1$ for $\varepsilon_a < \varepsilon_c$—the agreement is acceptable for a scaling assumption. For the smallest aspect ratio, $\varepsilon_a = 2/45$, β is almost an order of magnitude larger than α.

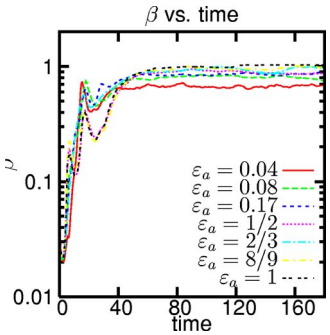

FIG. 7. As in Fig. 5, but for $\beta := \omega_h/\omega_z$.

06 July 2023 14:07:29

That the isotropization is incomplete for a finite range of ε_a should not be a surprise; after all, this is implied by the linear scaling (5). Nevertheless the persistence of the vortex tubes is remarkable. Although the real-space vorticity (potentially) exaggerates the importance of structures that are energetically weak, the perturbation vorticity does grow to fill the entire domain (cf. P1, Figs. 3 and 5). Since the vortices are narrow and tall one might expect them to be readily destroyed. Yet the flow does not isotropize immediately after the onset of saturation. The hyperbolic instability, which efficiently three-dimensionalizes the flow, in the sense of growth of 3D modes, does not leave the flow in an incipiently isotropic state.

VI. FEEDBACK ON THE BASE FLOW

The perturbation exerts a significant influence on the base flow. This is obvious from the vertically averaged vorticity fields of Fig. 6. In the absence of feedback effects the vertical vorticity contours would be undisturbed and the base flow dominated by a few coherent vortices; here, small-scale structure is conspicuous.

The total feedback may be estimated with the rms average of the base flow velocity, U_{rms}. The ensemble average, $\overline{U_{\mathrm{rms}}}$, decreases with ε_a (not shown), implying that the deceleration of the base flow (i.e., the damping) is greater for larger aspect ratios. The idea that the perturbation exerts a damping on the base flow, and that this damping increases with the aspect ratio, is developed below.

A. Transfer spectra

Transfer spectra quantify the scale dependence of the energy transfer. From the energy equation for the full 3D flow, one obtains

$$\mathcal{T}(k) := -\Re\left\{\sum_{|\boldsymbol{k}|=k} v_l(\boldsymbol{v}\cdot\boldsymbol{\nabla}\boldsymbol{v})_l^*(\boldsymbol{k})\right\}, \tag{7}$$

where the asterisk denotes complex conjugation, the 3D wave number $k=\sqrt{k_h^2+k_z^2}$, and l is a dummy index. Summation over repeated indices is implied. If $\mathcal{T}(k)>0$ then energy is injected into wave number k, whereas if $\mathcal{T}(k)<0$ energy is extracted from wave number k; $\mathcal{T}(k)=0$ in the inertial range. $\mathcal{T}(k_h)$ and $\mathcal{T}(k_z)$ are defined analogously. In a triply periodic domain

$$\sum_{k=0}^{K}\mathcal{T}(k)=\sum_{k_h=0}^{K_h}\mathcal{T}(k_h)=\sum_{k_z=0}^{K_z}\mathcal{T}(k_z)=0.$$

$\mathcal{T}(k)$ describes the total energy transfer. The energy transfer between the 2D base flow and the 3D perturbation can be quantified in the same way. The starting point is a closed set of equations for $\boldsymbol{u}$ and $\boldsymbol{U}$. Restoring hyperviscosity and nonlinearity

$$\begin{aligned}\frac{D\boldsymbol{u}}{Dt}&=-\boldsymbol{\nabla}p-\nu\nabla^8\boldsymbol{u}-\boldsymbol{u}\cdot\boldsymbol{\nabla}\boldsymbol{U}-(\boldsymbol{u}\cdot\boldsymbol{\nabla}\boldsymbol{u}-\widehat{\boldsymbol{u}\cdot\boldsymbol{\nabla}\boldsymbol{u}}),\\ \frac{D\boldsymbol{u}}{Dt}&=-\boldsymbol{\nabla}P-\nu\nabla^8\boldsymbol{U}-\widehat{\boldsymbol{u}\cdot\boldsymbol{\nabla}\boldsymbol{u}},\end{aligned} \tag{8}$$

the hat denoting a vertical average. These equations amount to a Reynolds-stress decomposition of the flow. In spectral space the associated energy equations are

$$\begin{aligned}\frac{D}{Dt}E_{3D}(k)=\sum_{|\boldsymbol{k}|=k}&[-ikp_l u_l^*-\nu k^8 u_l u_l^*-u_l(\boldsymbol{u}\cdot\boldsymbol{\nabla}\boldsymbol{U})_l^*(k)\\ &-u_l(\boldsymbol{u}\cdot\boldsymbol{\nabla}\boldsymbol{u}-\widehat{\boldsymbol{u}\cdot\boldsymbol{\nabla}\boldsymbol{u}})_l^*(k)],\\ \frac{D}{Dt}E_{2D}(k)=\sum_{|\boldsymbol{k}|=k}&[-ikP_l U_l^*-\nu k^8 U_l U_l^*-U_l(\widehat{\boldsymbol{u}\cdot\boldsymbol{\nabla}\boldsymbol{u}})_l^*(k)],\end{aligned} \tag{9}$$

where the perturbation energy $E_{3\mathrm{D}}(k)=\frac{1}{2}\Sigma_{|\boldsymbol{k}|=k}u_l u_l^*(\boldsymbol{k})$, the base-flow energy $E_{2\mathrm{D}}(k)=\frac{1}{2}\Sigma_{|\boldsymbol{k}|=k}U_l U_l^*(\boldsymbol{k})$, and the total energy $E(k)=E_{2\mathrm{D}}(k)+E_{3\mathrm{D}}(k)$. Thus, the effect of the perturbation on the base flow energetics is given by

$$\mathcal{T}_{3\mathrm{D}\to 2\mathrm{D}}(k_h) := -\Re\left\{\sum_{|\boldsymbol{k}_h|=k_h} U_l(\boldsymbol{u}\cdot\boldsymbol{\nabla}\boldsymbol{u})_l^*(\boldsymbol{k})\right\}, \tag{10}$$

where the sum is taken over a cylinder in spectral space. Likewise the transfer from the base flow to the perturbation via the production term,

$$\mathcal{T}_{2\mathrm{D}\to 3\mathrm{D}}(k_h) := -\Re\left\{\sum_{|\boldsymbol{k}_h|=k_h} u_l(\boldsymbol{u}\cdot\boldsymbol{\nabla}\boldsymbol{U})_l^*(\boldsymbol{k})\right\}, \tag{11}$$

and the purely 2D transfer

$$\mathcal{T}_{2\mathrm{D}\to 2\mathrm{D}}(k_h) := -\Re\left\{\sum_{|\boldsymbol{k}_h|=k_h} U_l(\boldsymbol{U}\cdot\boldsymbol{\nabla}\boldsymbol{U})_l^*(\boldsymbol{k})\right\}. \tag{12}$$

In this section we analyze $\mathcal{T}(k_h)$ and $\mathcal{T}_{3\mathrm{D}\to 2\mathrm{D}}(k_h)$ using data from the extended simulations of Fig. 5. Since the transfer spectra are noisy we apply a temporal average (a minimum of 62 samples for the early-time average, $t<t_{\mathrm{sat}}$, and 84 samples for the late-time average, $t>t_{\mathrm{sat}}$; $t_{\mathrm{sat}}=80$). This distinction between early and late times is arbitrary but convenient. For the most part the results are qualitatively similar; for brevity, only the late-time ones are shown. All the results in this section were obtained from the same basic state. Ensemble averages of extended simulations would be computationally expensive.

We begin with $\mathcal{T}(k_h)$. From Fig. 8, $\mathcal{T}(k_h)<0$ for small k_h while $\mathcal{T}(k_h)>0$ for large k_h. [For clarity we plot $k_h\mathcal{T}(k_h)$ and use log-linear axes so as to maintain area preservation.] In words, energy is extracted from large scales and injected into small scales. The sum over k_h is of the same order of magnitude as min $\mathcal{T}(k_h)$: there is no net transfer, as required.

Figure 8 suggests the existence of a forward energy cascade, such as in decaying 3D turbulence. Indeed, for $\varepsilon_a\leqslant\frac{1}{2}$ one can discern an "inertial range," for $5\lesssim k_h\lesssim 20$, in which $\mathcal{T}(k_h)\approx 0$. The inertial range is not as well defined at early times (not shown)—the fluctuations about $\mathcal{T}(k_h)=0$ are greater—but the picture is broadly similar. Since the flow is

06 July 2023 14:07:29

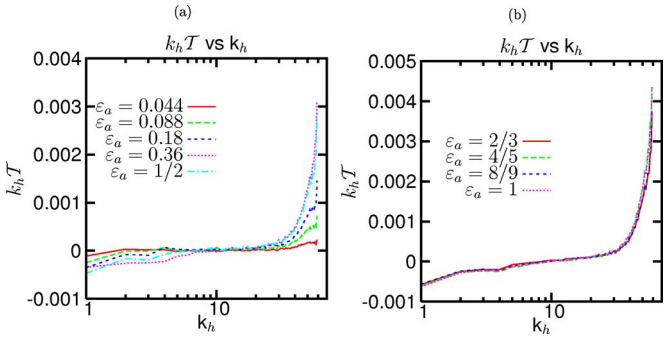

FIG. 8. $k_h\mathcal{T}$ vs k_h for different ε_a. (a) $\varepsilon_a \leqslant \frac{1}{2}$; (b) $\varepsilon_a > \frac{1}{2}$. Late-time behavior, $t \in [80,180]$. Each curve is obtained from temporal averaging. Data are taken from the simulations of Fig. 5. Note that the two panels have different vertical scales.

in the process of three-dimensionalizing for $t < t_{\text{sat}}$, the time-averaged transfer spectra are not stationary with respect to the averaging window.

The structure of the inertial range is independent of ε_a. But away from the inertial range the transfer depends on the aspect ratio: extraction from large scales and injection into small scales increase with ε_a. For larger aspect ratios there is an enhancement of the forward energy cascade—the magnitude of the transfer is greater. In agreement with the ensemble-averaged saturation level, the enhancement continues up to $\varepsilon_a \sim \varepsilon_c$ [compare panels (a) and (b)].

An enhanced forward cascade is more easily seen with normalized dissipation statistics. Defining

$$\mathcal{D}_{2D} := \frac{1}{\mathcal{D}_{\text{tot}}} \sum_{\boldsymbol{k}} k^8 E_{2D}(\boldsymbol{k}),$$

$$\mathcal{D}_{3D} := \frac{1}{\mathcal{D}_{\text{tot}}} \sum_{\boldsymbol{k}} k^8 E_{3D}(\boldsymbol{k}), \quad \mathcal{D}_{\text{tot}} := \sum_{\boldsymbol{k}} k^8 E(\boldsymbol{k}), \tag{13}$$

$\mathcal{D}_{2D}$ and $\mathcal{D}_{3D}$ characterize the forward cascade. For decaying, homogeneous turbulence $\mathcal{D}_{2D}=1$ and $\mathcal{D}_{3D}=0$ in 2D, while $\mathcal{D}_{2D} \approx 0$ and $\mathcal{D}_{3D} \to 1$ in 3D. Figure 9 shows $\mathcal{D}_{2D}$ and $\mathcal{D}_{3D}$ corresponding to the transfer spectra of Fig. 8. At least up to $\varepsilon_a \sim \varepsilon_c$, the 3D energy dissipation increases while the 2D energy dissipation decreases. In other words, there is an enhancement of the forward energy cascade for $\varepsilon_a \leqslant \varepsilon_c$: as

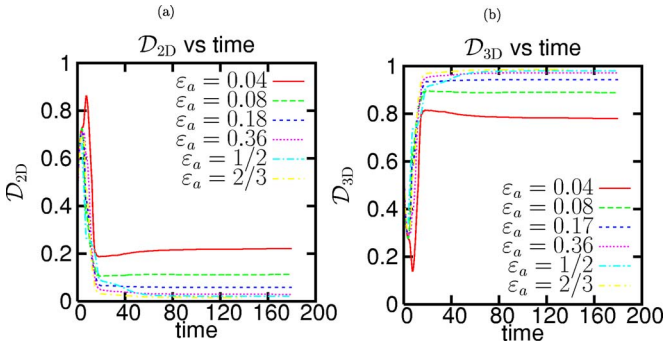

FIG. 9. Normalized dissipation statistics vs time for runs analyzed in Fig. 8. (a) $\mathcal{D}_{2D}$; (b) $\mathcal{D}_{3D}$.

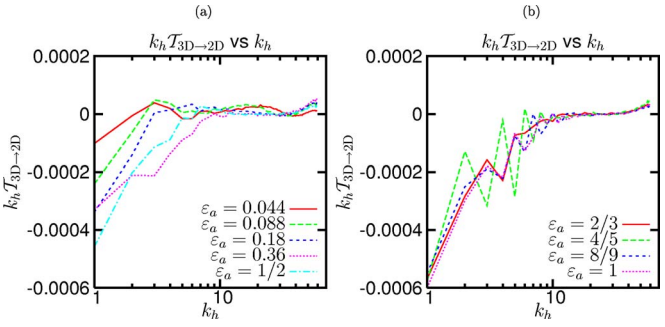

FIG. 10. As in Fig. 8, but for $\mathcal{T}_{3D\to 2D}$. (a) $\varepsilon_a \leqslant \frac{1}{2}$; (b) $\varepsilon_a > \frac{1}{2}$.

the vortex cores become progressively smaller, more energy is cascaded towards dissipation scales.

The feedback on the base flow, $\mathcal{T}_{3D\to 2D}$, is shown in Fig. 10. For $\varepsilon_a \leqslant \varepsilon_c$ the extraction of base-flow energy tends to increase with ε_a—the damping on the base flow is weaker in a thin domain. For $\varepsilon_a > \varepsilon_c$ the structure of $\mathcal{T}_{3D\to 2D}$ is more or less unchanged. The upshot is that the perturbation exerts a net damping on the base flow: $\Sigma_{k_h}\mathcal{T}_{3D\to 2D}(k_h) < 0$ for all ε_a. Indeed the damping scales approximately linearly with ε_a for $\varepsilon_a \leqslant \varepsilon_c$ (Fig. 11), that is, the feedback of the perturbation upon the base flow is directly proportional to the aspect ratio. The scaling breaks down for $\varepsilon_a > \varepsilon_c$, presumably on account of deviations from linear scaling of the saturation level (cf. Fig. 3). A linear damping is also obtained using ensemble-averaged data (not shown).

These results are consistent with the behavior of forced, rotating turbulence[6]: large-scale 2D modes extract less energy at small ε_a. Nonetheless they may be questioned because the end state of the three-dimensionalization typically consists of a pair of large vortices (cf. Fig. 6). However, with a random basic state in which the initial kinetic energy is confined to a narrow band between wave numbers 5 and 6, the structure of $\mathcal{T}_{3D\to 2D}$ is similar (Fig. 12). At early times the previous picture (Fig. 8) is recovered after the origin is shifted: because the energy is initially localized at large scales ($k_h \sim 5$) extraction occurs for smaller scales ($5 \lesssim k_h \lesssim 10$).

Apart from the aspect-ratio dependence, the spectral structure of $\mathcal{T}_{3D\to 2D}$ deserves comment. As with the total transfer (Fig. 8), there is extraction of base-flow energy

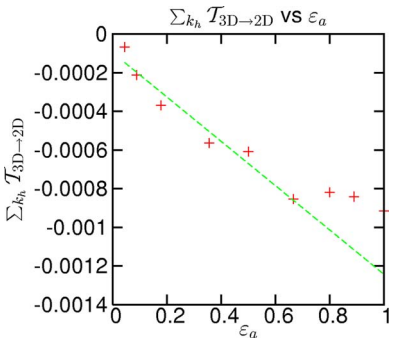

FIG. 11. $\Sigma_{k_h}\mathcal{T}_{3D\to 2D}$ vs ε_a. Data taken from Fig. 10. Points for which $\varepsilon_a > \frac{1}{2}$ are excluded from the least-squares fit.

06 July 2023 14:07:29

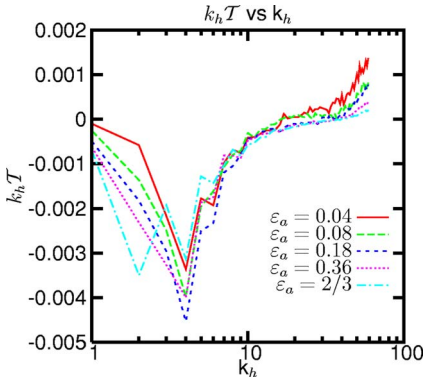

FIG. 12. $\mathcal{T}_{3D\to 2D}$ vs k_h for a random basic state. Time-averaged results for $t<20$.

($\mathcal{T}_{3D\to 2D}<0$) at large scales, and weak injection at small scales, though $\mathcal{T}_{3D\to 2D}\approx 0$ for $k_h \gtrsim 10$ after averaging from $t=80$ to $t=360$ (not shown). The key point is that the 2D modes that lose energy can be distinguished from the ones that do not. Despite some imprecision in the definition of the crossover wave number, which increases towards $k_h=10$ as ε_a is increased, it seems fair to conclude that the crossover occurs at $k_h \sim 10$. This behavior is also observed in extended long-time simulations.

The spectral structure of $\mathcal{T}_{3D\to 2D}$ can be understood by appealing to the 2D and 3D energy spectra, $E_{2D}(k)$ and $E_{3D}(k)$ (Fig. 13). For each ε_a, the 2D spectra shallow and the 3D spectra steepen at small scales, while the opposite occurs at large scales. Defining a wave number, k_{cross}, as the point where the 2D and 3D spectra intersect, 2D energy is lost for $k_h<k_{cross}$ but gained for $k_h>k_{cross}$ (and vice versa for the 3D energy). This has immediate implications for $\mathcal{T}_{3D\to 2D}$. One

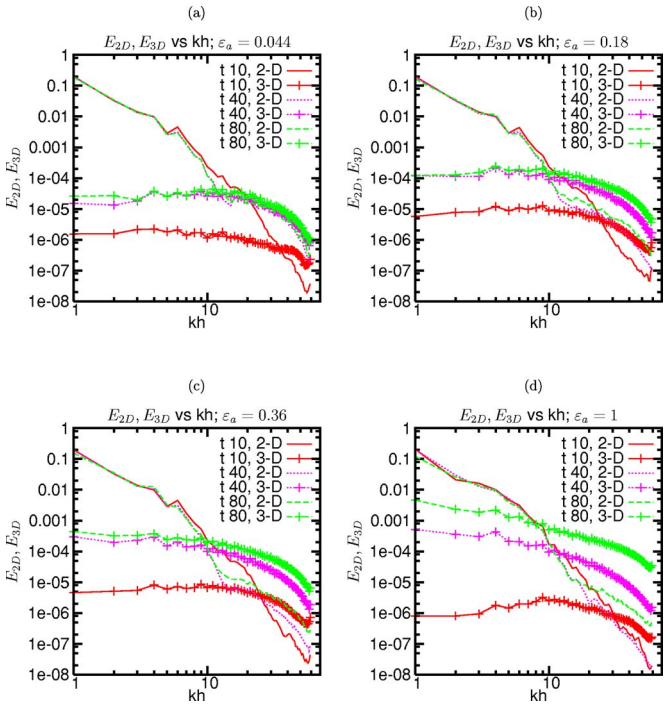

FIG. 13. 2D and 3D energy spectra for different ε_a. (a) $\varepsilon_a=0.044$ (b) $\varepsilon_a=0.18$; (c) $\varepsilon_a=0.36$; (d) $\varepsilon_a=1$.

expects k_{cross} to divide modes for which there is extraction, $\mathcal{T}_{3D\to 2D}<0$, from ones for which there is weak injection, $\mathcal{T}_{3D\to 2D}>0$, or even no net transfer, $\mathcal{T}_{3D\to 2D}\approx 0$ (cf. Fig. 10). As the perturbation grows the 3D spectra shift towards higher energies and k_{cross} migrates towards smaller wave numbers. For $\varepsilon_a<\varepsilon_c$ a "fixed point" is reached, whereas for $\varepsilon_a>\varepsilon_c$ the migration continues to smaller scales. $k_{cross}\sim 10$ for $\varepsilon_a<\varepsilon_c$ and $N_h=180$ (Fig. 13).

k_{cross} cannot be automatically associated with the $\mathcal{T}_{3D\to 2D}$ crossover wave number in Fig. 10. There is some ε_a dependence in the latter while k_{cross} varies for $\varepsilon_a>\varepsilon_c$. Nevertheless, the agreement is striking. At lower resolution ($N_h=120$ and $N_h=72$) E_{2D} and E_{3D} intersect, and $\mathcal{T}_{3D\to 2D}$ changes sign, at $k_{cross}\sim 10$. Likewise, the value of k_{cross} is the same for second- and third-order hyperviscosity, and even Laplacian viscosity (when there is sufficient vertical resolution). Evidently k_{cross} is determined by properties of the basic state.

This behavior is reminiscent of geophysical turbulence, in which the unbalanced modes feedback onto the balanced modes. In numerical simulations, the kinetic energy spectrum flattens out due to the interactions between the balanced and unbalanced modes[15–17]: there is a downscale cascade of wave energy. Here the feedback is simpler—the 2D and 3D modes can be defined unambiguously—but the basic idea remains the same. The base flow provides the energy for the perturbation, and is in turn subjected to a nonlinear feedback from the perturbation.

As ε_a is increased $E_{3D}(k)$ eventually steepens at small k_h, though it remains shallower than $E_{2D}(k)$. For this to occur, the rate at which energy is injected into the 3D modes must exceed the rate at which it is cascaded towards larger k_h. According to the pressureless analysis, the growth rate of the 3D perturbation is approximately independent of ε_a (cf. Fig. 1), but associated with large scales in an isotropic domain.

The transfer of energy from the base flow to the perturbation is quantified with $\mathcal{T}_{2D\to 3D}$. Figure 14 shows that while the structure of $\mathcal{T}_{3D\to 2D}$ changes noticeably with ε_a—the initial peak decreases in amplitude and shifts location—$\mathcal{T}_{2D\to 3D}$ is less sensitive to ε_a. Despite the redistribution of energy in spectral space—$\mathcal{T}_{2D\to 3D}$ is not a mirror image of $\mathcal{T}_{3D\to 2D}$—the total energy lost by the base flow approximately equals the energy gained by the perturbation, as it must. Within an error of 0.1%, $\Sigma_0^{K_h}\mathcal{T}_{3D\to 2D}(k_h)+\Sigma_0^{K_h}\mathcal{T}_{2D\to 3D}(k_h)=0$.

$\mathcal{T}_{2D\to 3D}$ is derived from the production term, $-\boldsymbol{u}\cdot\boldsymbol{\nabla U}$, which underlies the pressureless analysis. One may therefore ask how the pressureless dynamics are reflected in $\mathcal{T}_{2D\to 3D}$. In Fig. 14, $\Sigma_{k_h}\mathcal{T}_{2D\to 3D}(k_h)>0$, i.e., transfer to the perturbation continues after the perturbation has saturated. Since the production term is associated with linear growth this may be surprising; however, random straining by the base flow (and thus transfer via the production term) should occur even after saturation so long as the flow remains quasi-2D. For $t>t_{sat}$ the energy transferred to the 3D modes supports the forward cascade of energy rather than the growth of the perturbation.

We have examined the transfer in physical space using snapshots of $-\boldsymbol{u}\cdot\widehat{\boldsymbol{\nabla u}}$, the vector force representing the effect

06 July 2023 14:07:29

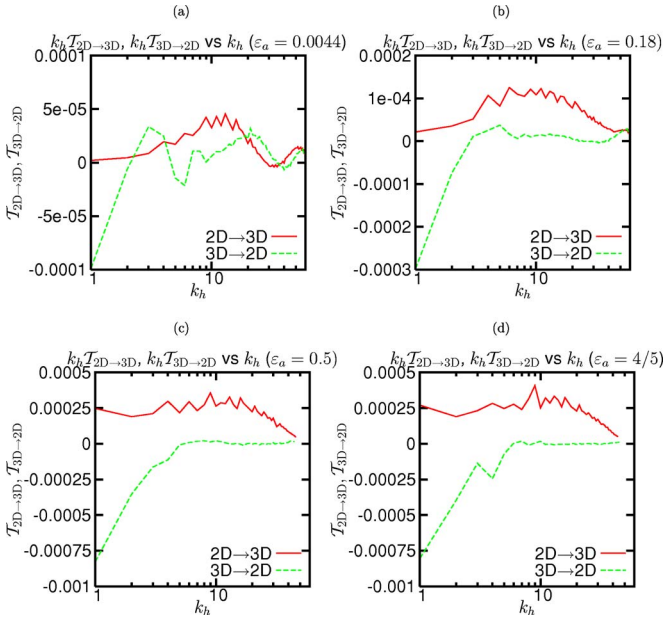

FIG. 14. As in Fig. 10 but for $\mathcal{T}_{2D\to3D}$ and $\mathcal{T}_{3D\to2D}$. (a) ε_a=0.044; (b) ε_a=0.18; (c) ε_a=1/2; (d) ε_a=4/5.

of the perturbation on the base flow momentum (not shown). During the linear stage of the growth, the magnitude of the force is largest in the vicinity of the "rib vortices" that emerge between the vortex tubes. Furthermore, the force tends to point in a direction parallel to them. After saturation it is difficult to discern any structure in $-\boldsymbol{u}\cdot\widehat{\boldsymbol{\nabla u}}$, even for the smallest ε_a.

From the preceding discussion, the following picture of the energy transfer emerges: 2D energy is extracted from the base flow and transferred to the 3D perturbation (Fig. 14), damping large scales (Fig. 10) before being cascaded forward towards dissipation scales (Fig. 8). This picture is supported by calculations of the purely 2D transfer, $\mathcal{T}_{2D\to2D}$ (not shown). For sufficiently large ε_a there is no sign of a forward cascade of 2D energy, and no real inverse cascade either.

B. Eddy viscosity

$\mathcal{T}_{3D\to2D}(k_h)$ represents the effect of the 3D perturbation on the 2D base flow. For applications, however, it is convenient to recast this information in terms of an eddy viscosity. In subgrid scale modeling the eddy viscosity encapsulates the effect of the unresolved scales on the resolved scales.[8,9] This procedure is easily adapted to the feedback of a 3D perturbation upon a 2D base flow. In the general case one considers the evolution of the resolved modes in terms of triad interactions with the resolved and unresolved modes, i.e., both resolved-unresolved-unresolved and resolved-resolved-unresolved interactions.[8,9] In the present case the problem simplifies. Since resolved modes are associated with $\boldsymbol{U}$ and the unresolved modes with $\boldsymbol{u}$, there is no need to consider resolved-resolved-unresolved interactions.

The eddy viscosity models the unresolved terms in the momentum equation (of the base flow) as $\nu_{eddy}\nabla^2\boldsymbol{U}$. An expression for the eddy viscosity—or more generally, effective viscosity—can be obtained by comparing $-\nu_{eddy}k_h^2U_lU_l^*$ to the unresolved terms in the energy equation. For

$$\frac{DE_k}{Dt}=\sum_i \mathcal{N}_u^i+\mathcal{N}_r^i,$$

where $\mathcal{N}_u^i$ and $\mathcal{N}_r^i$ label the unresolved and resolved terms, respectively, one gets

$$\nu_{eddy}^i := -\frac{\mathcal{N}_u^i}{k_h^2U_lU_l^*}.$$

The effective viscosity arising from the ∇^8 hyperviscosity operator then takes the form $\nu_{hyp}=\nu k_h^6$, while the eddy viscosity associated with the perturbation is

$$\nu_{eddy}(k_h)=-\sum_{|\boldsymbol{k}_h|=k_h}\frac{-U_l(\boldsymbol{u}\cdot\widehat{\boldsymbol{\nabla u}})_l^*(\boldsymbol{k})}{|\boldsymbol{\Omega}|^2(\boldsymbol{k})},\tag{14}$$

where $\boldsymbol{\Omega}$ is the 3D base-flow vorticity. Although the eddy viscosity is closely related to $\mathcal{T}_{3D\to2D}(k_h)$ [cf. (10)], ν_{eddy} is more conveniently employed in a parametrization.

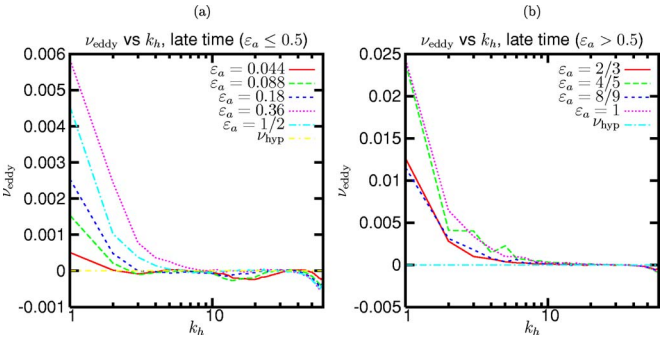

FIG. 15. ν_{eddy} vs. k_h for runs analyzed in Fig. 14. (a) $\varepsilon_a \leqslant 1/2$; (b) $\varepsilon_a > 1/2$. $t\in[80,180]$. For reference ν_{hyp} is also plotted.

Figure 15 plots ν_{eddy} against k_h for the runs analyzed in Fig. 10. For $\varepsilon_a \leqslant \frac{1}{2}$ [panel (a)], transfer from the 2D modes at small k_h yields a positive eddy viscosity, while transfer to the 3D modes at large k_h yields a negative eddy viscosity. Here the positive eddy viscosities, which swamp ν_{hyp}, may be associated with large-scale anisotropy. For $\varepsilon_a > \varepsilon_c$ the eddy viscosities remain negative for $k_h \gtrsim 10$, albeit small. In this range of ε_a the same structure is maintained: $k_h \approx 10$ demarcates the transition between positive and negative eddy viscosities. This behavior is analogous to that of $\mathcal{T}_{3D\to2D}$. Thus $\nu_{eddy}>0$ for $k_h<k_{cross}$ while $\nu_{eddy}\approx 0$ for $k_h>k_{cross}$. For $\varepsilon_a=1$ ν_{eddy} decreases by about two orders of magnitude from the largest to smallest scales.

The approximate self-similarity of the eddy viscosity suggests that the effects of the perturbation upon the base flow can be parametrized straightforwardly. One could take $\nu_{eddy}\approx 0$ for $k_h>k_{cross}$ and adopt a simple scaling for $k_h<k_{cross}$. For example, $\Sigma_{k_h=1}^{k_h=k_{cross}}\nu_{eddy}$ scales approximately linearly with ε_a, at least up to $\varepsilon_a=\frac{1}{2}$ (not shown).

The eddy viscosities of Fig. 15 are qualitatively different from those conventionally used in subgrid scale modeling. For isotropic 3D turbulence,[18,19] as well as rotating stratified turbulence,[10] there is a "cusp" for $k\to k_{cut}$, where k_{cut} is the

06 July 2023 14:07:29

cutoff scale for the resolved modes. Here the situation is different because the unresolved modes correspond to the 3D or $|k_z|>0$ modes. Since ν_{eddy} is computed as a function of k_h, no cusp is observed. Our eddy viscosity represents the correction to an idealized model, not to one with insufficient resolution.

VII. SUMMARY

This paper has shown that the three-dimensionalization of freely decaying two-dimensional turbulence is profoundly influenced by the aspect ratio of the domain, ε_a. While the linear growth rates are unaffected (as in the isotropic case, estimates can be obtained from a pressureless analysis), the aspect ratio has a significant effect on the long-time behavior, i.e., on the saturation level of the perturbation, $\boldsymbol{u}$, and its feedback on the base flow, $\boldsymbol{U}$.

First, the amplitude of the perturbation in the long-time limit, i.e., the saturation level, is determined by ε_a, in agreement with a simple scaling theory based on a matching of time scales between the 2D and 3D motion. The ensemble average, $\overline{u_{\text{sat}}}$, scales linearly with ε_a up to $\varepsilon_a \sim \frac{1}{2}$, the location of the "shoulder" at ε_c likely following from anisotropy in the base flow. With a pair of quasi-2D vortices $\varepsilon_c=\frac{1}{2}$ defines the aspect ratio for which the maximum saturation level is attained. The linear scaling and the value $\varepsilon_c=\frac{1}{2}$ are robust: they are also obtained using a more intermittent basic state, with an anisotropic grid, and at lower resolution. We have confirmed that the 2D and 3D time scales are comparable after saturation occurs, i.e., $\omega_h/\omega_z \sim 1$.

Survival of the quasi-2D vortices leads to significant anisotropy of the flow. From long extended simulations and short ensemble runs, complete isotropization does not occur for $\varepsilon_a \leqslant \varepsilon_c=\frac{1}{2}$ (at least on the time scales examined). The "return to isotropy" is extremely slow for $\varepsilon_a>\varepsilon_c$, complete isotropization requiring several hundred eddy turnover times; but in agreement with phenomenological theories and closure calculations, there appears to be exponential relaxation towards $\alpha=1$.[3,13,14]

It makes sense that the same critical threshold, $\varepsilon_a=\varepsilon_c$ should apply to the scaling of the saturation level and the isotropization of the flow. The saturation level is maximized when the flow is completely isotropized. Unfortunately, however, it isn't exactly clear why $\varepsilon_c=\frac{1}{2}$ should define a critical threshold, though the fact the characteristic 2D wave number $k_{2\text{D}} \sim 2$ does support our claim. While the vortices should be more susceptible to 3D instabilities when $\varepsilon_a>\frac{1}{2}$, this says nothing about the details of the isotropization. Even so, the existence of this critical threshold, which appears to be independent of the perturbation amplitude and the basic state, is noteworthy.

Second, the perturbation exerts a net damping effect on the base flow. This damping manifests itself through the time-averaged transfer function, $\mathcal{T}_{3\text{D}\to 2\text{D}}: \Sigma_{k_h}\mathcal{T}_{3\text{D}\to 2\text{D}}<0$. Furthermore, $\Sigma_{k_h}\mathcal{T}_{3\text{D}\to 2\text{D}}$ scales linearly with ε_a up to $\varepsilon_a=\frac{1}{2}$. This is the most significant outcome of the energy transfers between the 2D and 3D modes. In general, there is an enhanced forward energy cascade for larger ε_a, and the transfer from the base flow to the perturbation, $\mathcal{T}_{2\text{D}\to 3\text{D}}$, continues after the perturbation has saturated.

In spectral space the effects of the perturbation on the base flow assume a simple form. Reexpressing $\mathcal{T}_{3\text{D}\to 2\text{D}}$ as an eddy viscosity, $\nu_{\text{eddy}}>0$ for $k_h<10$ and $\nu_{\text{eddy}}\approx 0$ for $k_h>10$. The crossover wave number $k_{\text{cross}}=10$ appears to be associated with the 2D and 3D energy spectra. For $k_h<k_{\text{cross}}$ the 2D energy dominates, whereas for $k_h>k_{\text{cross}}$ the 3D energy dominates.

These results could be applied to a parametrization of subgrid-scale mixing. Since the eddy viscosity is small for large k_h, the parametrization problem might not be so difficult: low-resolution data may suffice. Furthermore, $\nu_{\text{eddy}}(k_h)$ is approximately self-similar. With knowledge of $E_{2\text{D}}$, $E_{3\text{D}}$, and $\mathcal{T}_{3\text{D}\to 2\text{D}}$, one may be able to parameterize ν_{eddy} as a function of k_h. Such a procedure would be valuable in the modeling of large-scale geophysical flows.

ACKNOWLEDGMENTS

Helpful comments were received from an anonymous reviewer. Financial support was provided by NSERC and the Canadian Foundation for Climate and Atmospheric Science. Computational resources were provided by CLUMEQ.

[1] K. Ngan, D. N. Straub, and P. Bartello, "Three-dimensionalization of freely-decaying two-dimensional turbulence," Phys. Fluids **16**, 2918 (2004).
[2] D. N. Straub, "Instability of 2D flows to hydrostatic 3D perturbations," J. Atmos. Sci. **60**, 79 (2003).
[3] S. B. Pope, *Turbulent Flows* (Cambridge U.P., Cambridge, 2000).
[4] M. Lesieur, *Turbulence in Fluids*, 2nd ed. (Kluwer, Dordrecht, 1989).
[5] L. M. Smith, J. R. Chasnov, and F. Waleffe, "Crossover from two- to three-dimensional turbulence," Phys. Rev. Lett. **77**, 2467 (1996).
[6] L. M. Smith and F. Waleffe, "Transfer of energy to two-dimensional large scales in forced, rotating three-dimensional turbulence," Phys. Fluids **11**, 1608 (1999).
[7] J. Pedlosky, *Geophysical Fluid Dynamics*, 2nd ed. (Springer, New York, 1987).
[8] J. A. Domaradzki, R. W. Metcalfe, R. S. Rogallo, and J. J. Riley, "Analysis of subgrid-scale eddy viscosity with use of results from direct numerical simulations," Phys. Rev. Lett. **58**, 547 (1987).
[9] J. A. Domaradzki, W. Liu, and M. E. Brachet, "An analysis of subgrid-scale interactions in numerically simulated isotropic turbulence," Phys. Fluids A **5**, 1747 (1993).
[10] P. Bartello, O. Métais, and M. Lesieur, "Geostrophic versus wave eddy viscosities in atmospheric models," J. Atmos. Sci. **53**, 564 (1996).
[11] T. G. Shepherd, "Rigorous bounds on the nonlinear saturation of instabilities to parallel shear flow," J. Fluid Mech. **196**, 296 (1988).
[12] The thinnest domain corresponds to $\varepsilon_a=8/180$ or $\varepsilon_a \approx 0.044$.
[13] J. R. Herring, "Approach of axisymmetric turbulence to isotropy," Phys. Fluids **17**, 859 (1974).
[14] U. Schumann and J. R. Herring, "Axisymmetric homogeneous turbulence: a comparison of direct spectral simulations with the direct-interaction approximation," J. Fluid Mech. **76**, 765 (1976).
[15] P. Bartello, "Geostrophic adjustment and inverse cascades in rotating stratified turbulence," J. Atmos. Sci. **52**, 4410 (1995).
[16] J. N. Koshyk, K. Hamilton, and J. D. Mahlman, "Simulations of the $k^{-5/3}$ mesoscale spectral regime in the GFDL SKYHI general circulation model," Geophys. Res. Lett. **26**, 843 (1999).
[17] T. G. Shepherd, J. N. Koshyk, and K. Ngan, "On the nature of large-scale mixing in the stratosphere and mesophere," J. Geophys. Res. **105**, 12433 (2000).
[18] R. H. Kraichnan, "Eddy viscosity in two and three dimensions," J. Atmos. Sci. **29**, 1041 (1972).
[19] M. Chollet and M. Lesieur, "Parameterization of small scales of three-dimensional isotropic turbulence utilizing spectral closures," J. Atmos. Sci. **38**, 2747 (1981).

06 July 2023 14:07:29